



## City Research Online

### City, University of London Institutional Repository

---

**Citation:** Nadimi, S., Fonseca, J., Bésuelle, P. and Viggiani, G. (2015). A microstructural finite element analysis of cement damage on Fontainebleau Sandstone. Paper presented at the ICTMS 2015, 2nd International Conference on Tomography of Materials and Structures, 29 Jun - 3 Jul 2015, Québec, Canada.

This is the accepted version of the paper.

This version of the publication may differ from the final published version.

---

**Permanent repository link:** <https://openaccess.city.ac.uk/id/eprint/12317/>

**Link to published version:**

**Copyright:** City Research Online aims to make research outputs of City, University of London available to a wider audience. Copyright and Moral Rights remain with the author(s) and/or copyright holders. URLs from City Research Online may be freely distributed and linked to.

**Reuse:** Copies of full items can be used for personal research or study, educational, or not-for-profit purposes without prior permission or charge. Provided that the authors, title and full bibliographic details are credited, a hyperlink and/or URL is given for the original metadata page and the content is not changed in any way.

---

---

---

City Research Online:

<http://openaccess.city.ac.uk/>

[publications@city.ac.uk](mailto:publications@city.ac.uk)

---

# A microstructural finite element analysis of cement damaging on Fontainebleau Sandstone

S. NADIMI<sup>1</sup>, J. FONSECA<sup>\*1</sup>, P. BESUELLE<sup>2</sup>, G. VIGGIANI<sup>2</sup>

<sup>1</sup> City University London, UK  
<sup>2</sup> Laboratoire 3SR, Grenoble, France  
\* presenting author

**Keywords:** Microstructure of soil, tomography, sandstone, image,  $\mu$ FE, finite element modelling

## Abstract

This paper presents a numerical simulation that uses tomographic data to reproduce the grain-scale mechanisms taking place during deformation of Fontainebleau sandstone. Previous investigation using x-ray tomographic images acquired during triaxial compression has highlighted the role of bonding rupture mechanisms in the failure mode of the material. The model the deformation of the sandstone, images of the internal topology were used to generate an image-based finite element mesh and the grain-scale phenomena such as, the opening and propagation of the cracks associated with the debonding of the cemented grains, were reproduced using a simple constitutive model.

## Introduction

Fontainebleau (FB) sandstone from the Paris basin in France is a quartzitic sandstone with a median grain size of  $260\mu\text{m}$  and a degree of cementation that can vary considerably (Thiry and Maréchal, 2001). These differences in the amount of cement in the specimen lead to notable distinct microstructures and consequently significantly different failure mechanisms. Fonseca et al. (2013) has investigated the grain-scale deformation mechanisms associated with a soft FB specimen with 21% porosity and a very hard, tightly cemented sandstone with 6% porosity. This study highlighted the role of bonding rupture mechanisms to explain the differences in behaviour between the soft and the hard FB sandstone. Using tomographic data of the full specimen under triaxial compression, axial splitting was observed to occur in the sample shortly after 2% axial deformation, as a consequence of tensile failure at the grain-to-grain cemented interface. The grain-scale phenomena was observed to involve progressive contact damaging or 'cracking' leading to the debonding of the cemented contacts. This process eventually coalesced into larger geometrical discontinuities or 'vertical ridges', which resulted in the formation of vertical columns of horizontally unbonded grains able to transfer stresses along the direction of the major principal stress.

In the past decades, the reconstruction of microstructure of natural porous rock has become of increasingly interest for the petroleum industry and a number of numerical approaches have been proposed (Tacher et al. 1997; Yeong and Torquato, 1998; Pilotti, 1998; Jin et al. 2003; Holtzman, 2012). Stochastic reconstruction is an example of a commonly used approach. It consists of matching the statistical properties of a model to those of the microstructure to simulate the relevant physical processes of a rock formation, such as, sedimentation, compaction and diagenesis (Yeong and Torquato, 1998; Jin et al. 2004). The computational effort for microstructure reconstruction, which is the first stage to investigate the mechanical behaviour of geomaterials, raises with the complexity of the depositional method adopted and represents, generally, the lengthier part of the simulation.

In the present paper, a microstructural finite element ( $\mu$ FE) model which combines x-ray micro-computed tomography data with finite element analysis is developed. It follows on Nadimi et al. (2015) work to simulate the grain-to-grain interaction in an uncemented sand. The present study enables numerical simulation of the tightly cemented FB specimen that accounts for the microstructural features, such as, the geometrical arrangement of the grains and pores, grain shape and contact topology including degree and spatial distribution of the cement.

## Methodology

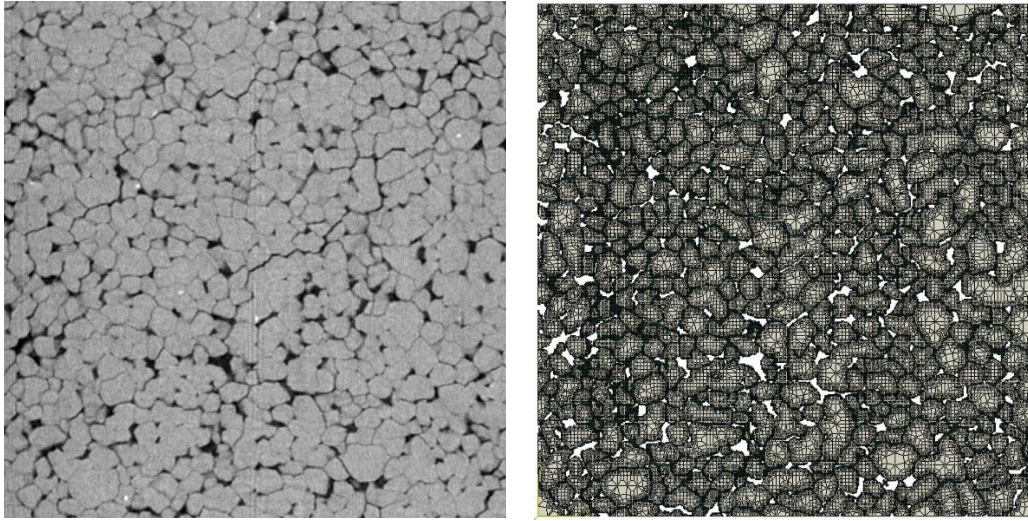
The  $\mu$ FE model proposed in this paper uses a finite element mesh produced from a two-dimensional (2D) image containing all the geometrical microstructural information. The input data for the  $\mu$ FE model was obtained in three key stages: image acquisition and image segmentation, image-based meshing and constitutive modelling, as described in this Section.

### *Image acquisition and segmentation*

Non-invasive images of the initial microstructure of FB sandstone were acquired using high resolution x-ray computed tomography ( $\mu$ CT). The images have a spatial resolution of  $8.5\mu\text{m}$ , i.e.  $0.033 \times d_{50}$ , which allows the identification of the constituent microstructural features, such as, the grains, pore space and cement. As shown in Figure 1a, the pixels representing the grains, or solid phase, have brighter color (denser material) while the pore space is associated with darker pixels. The cement is essentially formed of quartz overgrowths, which complicates the dissociation between cement and quartz grains, however, it was observed that in general the cement is usually darker than the grains. An intensity-based threshold technique was used to classify (or segment) the three phases, i.e. solid grains, void space and cemented contacts. The obtained segmented image was the starting point to develop the image-based mesh.

### *Image-based meshing*

An open source software package OOF2 (Object Oriented Finite Elements v2, NIST) was used to create the mesh directly from the image (Reid et al. 2008). A simple and straightforward way to generate the mesh is using a direct pixel-to-element approach. However, the computational costs of running the model can be very high for large images. A more efficient approach is proposed here, which assumes that the grains are homogenous and therefore each grain can be represented by larger elements containing more than one pixel. These elements can be defined by various polygonal shapes, for which the size and shape depend on the size and shape of the respective grain. Using this approach, the initial mesh was defined according to the geometrical characteristics of each grain. The correction of the elements containing more than one phase can be carried out by either subdividing the elements, which increases the number of elements, or running a routine that changes the topology of element without increasing the number of elements. In this routine, nodes can be added, removed or reconnected to increase the homogeneity of the mesh. The assessment of the quality and efficiency of the mesh was taken into account by quantifying i) the ability of the mesh to represent the features in the images, using the *homogeneity index*, and ii) the mesh convergence behaviour, using the *shape index*. In the case of all the pixels in the image being associated to a mesh element, the *homogeneity index* equals 1. The *shape index* of regular shaped elements, such as triangles and squares equals 0, while the *shape index* of thin and elongated elements takes higher values. Following the necessary corrections and improvements of the mesh, it was subsequently imported to the finite element code.



(a)

(b)

**Fig. 1.** a)  $\mu$ CT raw image; b) Image-based Finite Element mesh, elements representing the bonding between grains contain smaller elements and are shown in darker colour.

### *Constitutive model*

Following observations from Fonseca et al. (2013), it is assumed that the deformation of the material is governed by bond rupture, thus, representation of this cracking and post cracking response are the key aspects in the modelling. The simulation of bonding damage and crack formation was carried out by using a constitutive model which takes the cracking response into finite element calculations.

Cracking was modelled by assigning a smeared cracking constitutive model to the cement (Belytschko et al. 1988; Borst et al. 2004). By using this constitutive model, cracks remain for the full finite element calculation and may open or close. The presence of cracks enters into this calculation by the way in which the crack affects the current strength and stiffness associated with the integration point. It is considered that a crack is initiated when the stress at an integration point satisfies a specified condition, e.g. the major principal stress reaching the tensile strength. The initial small cracks tend to connect to form one, or more than one, dominant crack, as deformation progresses.

### **Numerical Model**

This  $\mu$ FE model consists of a 2D array of approximately 560 grains subjected to triaxial compression. A segmented image with a size of 680  $\times$  700 pixel was used to generate the mesh. Mesh enhancement and refinement, resulted in a *homogeneity index* of 0.94 and a *shape index* of 0. In total, it comprised 126,923 nodes and 121,389 elements as shown in Figure 1b. The image-based mesh was imported into a commercial finite element package, Abaqus v6.13 (Dassault Systèmes). In order to simulate triaxial compression conditions, the bottom and left boundaries were fixed in the normal direction and 2MPa isotropic compression was applied to the top and to the right boundaries, in the first step, in order to reproduce the experimental conditions (Figure 2a). Axial loading was subsequently applied by defining a prescribed displacement at the top of the model, up to about 4% axial strain (Figure 2b), this was the point at which the deviatoric stress was seen to reach a plateau in the stress:strain experimental curve from Fonseca et al. (2013). The grain-to-grain contact interaction was simulated by assuming hard contact in the normal direction and Coulomb friction in the tangential

direction. Values of 100 GPa for Young's modulus and 0.15 for Poisson's ratio, corresponding to bulk modulus of  $K=47.6\text{GPa}$  and shear modulus of  $G=43.5\text{GPa}$ , were assigned to the grains. It was assumed that the cement has an Young's modulus of 30% of the grain's value and that the strain softening reduces the stress linearly to zero at a 0.5% strain after failure.

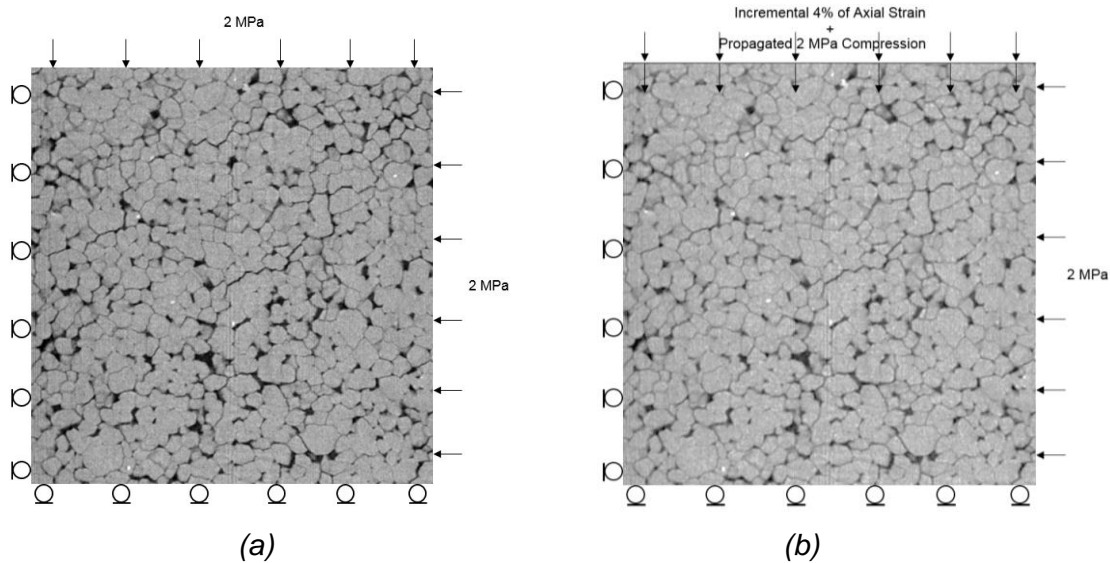


**Fig. 2.** Boundary conditions a) Stage 1: isotropic compression; b) Stage 2: incremental displacement.

## Results

The results were investigated in terms of maps of the stress and strain distribution. Figure 3a shows the formation of vertical columns of highly stressed grains, i.e. represented by brighter colours, which is in line with the experimental observations reported in Fonseca et al. (2013). The experimental data has shown that these columns are formed by horizontally unbonded grains following cement rupture along vertical ridges. In the present study, in order to investigate the cracking pattern, it was assumed that the direction of the minimum principal strain is parallel to the direction of cracking. The direction of the minimum principal strain is presented in Figure 3b by short arrows, which as expected, tend to exhibit a near vertical orientation. The strain distribution also presented in Figure 3b shows the higher strain concentration at the contacts between grains.

## Conclusion

The present paper contributes the first step towards the development of microstructure-informed numerical modelling of bonded geomaterials. The numerical approach proposed here uses a 2D image, of the internal microstructure of a tightly cemented sandstone, to reproduce the grain-scale phenomena observed to take place on real specimens investigated using tomographic data acquired at different stages of deformation. The results presented, although preliminary, clearly show the potential of this analysis to overcome some of the challenges associated with modelling the mechanical behaviour of cemented geomaterials to failure. Future work includes the 3D extension of this  $\mu\text{FE}$  model.

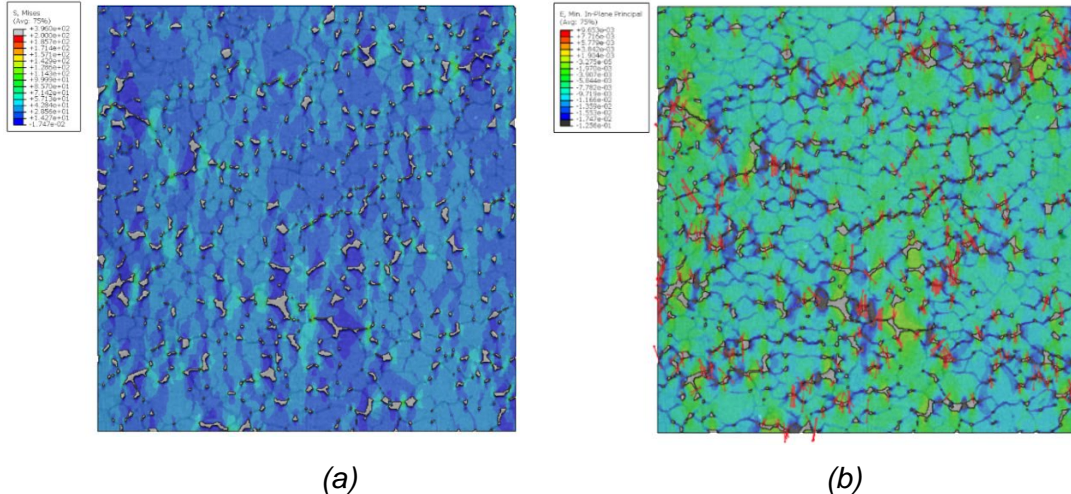


**Fig. 3.** a) Stress distribution map; b) Strain distribution map with arrows indicating the direction of the cracks in the cement given by the direction of the minimum principal strain.

## Acknowledgments

The authors would like to acknowledge the National Institute of Standards and Technology (NIST) for the code OOF2 used in this study.

## References

- Belytschko, T., Fish, J., Engelman, B.E. (1988) A finite element with embedded localization zones. *Computer Methods in Applied Mechanics and Engineering*, 70, 59-89.
- Borst, R., Remmers J.C., Needleman, A., Abellan M.A. (2004) Discrete vs smeared crack models for concrete fracture. *International Journal for Numerical and Analytical Method in Geomechanics*, 28,583-607.
- Fonseca, J., Besuelle, P. and Viggiani, G. (2013) Micromechanisms of inelastic deformation in sandstones: an insight using x-ray microtomography, *Geotechnique Letters* 3, No. 2, 78–83.
- Hillerborg, A., Modéer, M., Petersson, P.E. (1976) Analysis of crack formation and crack growth in concrete by means of fracture mechanics and finite elements, *Cement and Concrete Research*, 6, No. 6, 773-781.
- Holtzman, R. (2012) Micromechanical model of weakly-cemented sediments, *International Journal for Numerical and Analytical Method in Geomechanics* 36, 944-958.
- Jin, G., Patzek, T.W., Silin, D.B. (2004) *Dynamic reconstruction of sedimentary rock and simulation of its mechanical properties*, U.S. Department of Energy, LBNL-55038.
- Jin, G., Patzek, T.W., Silin, D.B. (2003). *Physics-based reconstruction of sedimentary rocks (SPE83587)*. SPE Western Regional/AAPG Pacific Section Joint Meeting, Long Beach, CA.
- Mourzenko, V.V., Thovert, J. F., Adler, P.M. (2001). Percolation in two-scale porous media, *The European Physical Journal B*, 19, No. 1, 75-85.
- Nadimi, S., Fonseca, J., Taylor, N. (2015). A microstructure-based finite element analysis of the response of sand, *6<sup>th</sup> Int. Sym. On Deformation Characteristics of Geomaterials*, Buenos Aires, Argentina.
- Pilotti, M. (1998) Generation of realistic porous media by grains sedimentation. *Transport in Porous Media*, 33, 257-278.
- Potyondy D.O., Cundall P.A. (2004). A bonded-particle model for rock. *International Journal of Rock Mechanics and Mining Sciences* 41, No. 8,1329–1364.
- Reid, A.C.E., Langer, S.A., Lua, R.C., Coffman, V.R., Haan, S., García, R.E. (2008). Image-based finite element mesh construction for material microstructures, *Computational Materials Science* 43, 989-999.
- Tacher, L., Perrochet, P., Parriaux, A. (1997) Generation of granular media. *Transport in Porous Media*, 26, 99-107.
- Thiry, M. and Marechal, B., (2001) Development of Tightly Cemented Sandstone Lenses in Uncemented Sand: Example of the Fontainebleau Sand (Oligocene) in the Paris Basin, *Journal of Sedimentary Research* 71, No. 3, 473-483.
- Yeong, C.L.Y., Torquato, S. (1998) Reconstructing random media. II. Three-dimensional media from two-dimensional cuts. *Physical Review B*, 58, No. 1, 224–233.